The Journal of Chemical Physics

Modeling the cholesteric pitch of apolar cellulose nanocrystal suspensions using a chiral hard-bundle model

Cite as: J. Chem. Phys. **156**, 014904 (2022); https://doi.org/10.1063/5.0076123
Submitted: 21 October 2021 • Accepted: 09 December 2021 • Accepted Manuscript Online: 13 December 2021 • Published Online: 04 January 2022

Massimiliano Chiappini, Simone Dussi, Bruno Frka-Petesic, et al.

The Journal of Chemical Physics ARTICLE scitation.org/journal/jcp

Modeling the cholesteric pitch of apolar cellulose nanocrystal suspensions using a chiral hard-bundle model

Cite as: J. Chem. Phys. 156, 014904 (2022); doi: 10.1063/5.0076123
Submitted: 21 October 2021 • Accepted: 9 December 2021 •
Published Online: 4 January 2022

Massimiliano Chiappini,[1] Simone Dussi,[2] Bruno Frka-Petesic,[3] Silvia Vignolini,[3] and Marjolein Dijkstra[1,a)]

AFFILIATIONS

[1] Soft Condensed Matter, Debye Institute for Nanomaterials Sciences, Utrecht University, Princetonplein 5, 3584 CC Utrecht, The Netherlands
[2] Physical Chemistry and Soft Matter, Wageningen University, Stippeneng 4, 6708 WE Wageningen, The Netherlands
[3] Melville Laboratory for Polymer Synthesis, Yusuf Hamied Department of Chemistry, University of Cambridge, Lensfield Road, Cambridge CB2 1EW, United Kingdom

[a)] **Author to whom correspondence should be addressed:** m.dijkstra@uu.nl

ABSTRACT

Cellulose nanocrystals (CNCs) are naturally sourced elongated nanocolloids that form cholesteric phases in water and apolar solvents. It is well accepted that CNCs are made of bundles of crystalline microfibrils clustered side-by-side, and there is growing evidence that each individual microfibril is twisted. Yet, the origin of the chiral interactions between CNCs remains unclear. In this work, CNCs are described with a simple model of chiral hard splinters, enabling the prediction of the pitch using density functional theory and Monte Carlo simulations. The predicted pitch $\mathscr{P}$ compares well with experimental observations in cotton-based CNC dispersions in apolar solvents using surfactants but also with qualitative trends caused by fractionation or tip sonication in aqueous suspensions. These results suggest that the bundle shape induces an entropy-driven chiral interaction between CNCs, which is the missing link in explaining how chirality is transferred from the molecular scale of cellulose chains to the cholesteric order.

I. INTRODUCTION

Due to its abundance, versatility, and environmental advantages over fossil-based resources, cellulose represents an important green resource that has stimulated intensive research activities on both fundamental and applied levels.[1] Among its surprising, yet poorly understood, properties is its occurrence in chiral assemblies within plant tissues,[2–4] providing adjustable mechanical resistance or structural color effects.[5] The ability of splinter-like cellulose nanocolloids, also known as cellulose nanocrystals (CNCs), to spontaneously form chiral nematic liquid crystal phases[6] suggests that this chiral behavior originates from cellulose itself rather than from biologically driven processes.[7–9] While the origin of the molecular chirality of cellulose is clear (cellulose is made of D-glucose, a chiral molecule), elucidating the transfer mechanisms of its chirality to its supramolecular level, from the microfibrils to the chiral suspensions,[10,11] has triggered much interest in the cellulose community and beyond.

Predicting the collective chiral behavior of the liquid crystalline state from the individual description of the molecular or colloidal constituents is a more general problem that presents its own technical challenges.[12–15] In the case of CNCs, this is further complicated by the fact that a simple but representative model of the individual CNCs is still missing. In most cases, CNCs are represented as achiral lath-like rods, as their twisted nature is usually only visible at the scale of microns of much longer CNCs.[16] Majoinen *et al.* employed electron tomography to visualize CNCs in 3D, demonstrating that CNCs form bundles with twisted shapes,[17,18] but their observations suffered from poor statistics. Therefore, the key parameters driving the chiral self-assembly of CNCs are still heavily debated.

In this regard, even a semi-quantitative theory that captures the main physical mechanism and predicts the twisting of the nematic

phase of CNCs, as described by its cholesteric pitch $\mathscr{P}$, in agreement with experimental observations, could shed light on the nature of the microscopic chirality of CNCs.

The mechanisms behind the spontaneous alignment of CNCs into (chiral) nematic liquid crystal phases can be explained by a trade-off between the rotational and translational entropy of the individual rods upon increasing the volume fraction, as demonstrated in the seminal work of Lars Onsager for systems of infinitely long rods,[19] which was later refined for rods with finite aspect ratios,[20,21] polydisperse rods,[22] electrostatic effects in aqueous media,[23–27] as well as for chiral deformations.[28] To account qualitatively for the formation of chiral nematic (or cholesteric) phases, additional chiral interactions were mostly considered, such as the corkscrew model in the limit of small twists.[29–31] This model suggests that CNCs are twisted parallelepipeds characterized by a microscopic pitch p that pack more efficiently when slightly tilted with respect to one another. In this way, rods may fit into the grooves of neighboring rods, thereby yielding a collective twist. This description accounts for the apparent reduction of the chiral interactions in water at low ionic strength, where large Debye screening lengths contribute to mask the chiral shape of the CNCs.[32] However, chiral nematic phases were also formed when the charges were neutralized or were unable to ionize and when the CNCs were stabilized with steric interactions using polymer grafting or surfactants.[33–35]

Recently, the first quantitative description of chiral self-assembly of CNCs in aqueous media was proposed by Kuhnhold *et al.* based on Monte Carlo (MC) simulations of helical Yukawa rods.[36,37] In their work, the CNCs were modeled as hard spherocylinders around which a set of discrete point charges was wrapped in a helical arrangement. However, a direct comparison of the simulated cholesteric pitch $\mathscr{P}$ as a function of thermodynamic state with experiments on CNC suspensions in aqueous media[11,27] is difficult as their *ad hoc* description of the chiral interactions of the CNCs cannot be connected to the existing experimental observations on the microscopic details of actual CNCs.

In this work, we quantitatively test the hypothesis that the self-assembly behavior of CNCs can be described by a system consisting of chiral hard splinters using both density functional theory (DFT) and Monte Carlo (MC) simulations.[15] We carefully design a model CNC shape that allows for a direct comparison with experimental observations and that accounts for the twisted microstructure of cellulose microfibrils described by a microscopic pitch p, the apparent CNC bundle structure, the effect of polydispersity, and the effect of surfactants on the effective shape and on the volume and mass fractions. Importantly, we postulate that the twisted structure of the individual microfibrils is only relevant to explain the twisted shape of the bundles and that the latter is the main driving mechanism to cause a twisted alignment of the bundles, resulting in a cholesteric phase. Hence, we model the individual microfibrils within each CNC as achiral hard spherocylinders, while the chirality of the resulting CNCs arises from the twist between adjacent microfibrils as described by the microscopic pitch p inherited from the individual microfibrils.

We show that this simple CNC model of chiral hard splinters stabilizes a cholesteric phase in agreement with Straley's theory and Onsager theory as well as simulations of chiral rods.[14,15,38,39] More importantly, we find that the predicted pitch qualitatively agrees with the experimental observations of cotton-based CNC dispersions in apolar solvents using surfactants and explains well certain trends of the variation of the cholesteric pitch caused by fractionation or tip sonication in aqueous suspensions.

II. METHODS

A. Density functional theory for chiral nematic phases

The stability of the cholesteric phase N^* and the equilibrium macroscopic pitch $\mathscr{P}$ was investigated by employing a classical density functional theory (DFT) for chiral nematic phases.[14,15,39] Here, we briefly describe the main points of this second-virial DFT approach and refer the interested reader to Refs. 14, 15, and 39. The main ingredient of the theory is the excluded volume between two particles separated by a (center-to-center) distance $\mathbf{r}$ with the orientation described by a 3×3 rotation matrix $\mathscr{R}$ and a corresponding unit vector $\hat{\mathbf{u}}$ denoting the orientation of the longest particle axis. The excluded volume depends on the (imposed) macroscopic chirality of N^*. In particular, the following Legendre polynomial expansion coefficients are calculated:

$$E_{ll'}(q) = -\int d\mathbf{r}\int d\mathscr{R}\, d\mathscr{R}'\, f(\mathbf{r},\mathscr{R},\mathscr{R}')P_l(\hat{\mathbf{n}}_q(z)\cdot\hat{\mathbf{u}})P_{l'}(\hat{\mathbf{n}}_q(0)\cdot\hat{\mathbf{u}}'), \tag{1}$$

where $q = 2\pi/\mathscr{P}$ is the inverse macroscopic pitch, $\hat{\mathbf{n}}_q(z) = \hat{\mathbf{x}}\sin(qz) + \hat{\mathbf{y}}\cos(qz)$ is the nematic director profile, and P_l is a normalized Legendre polynomial of degree l, where we consider up to $l = 20$. Furthermore, $f(\mathbf{r},\mathscr{R},\mathscr{R}')$ is the Mayer function between two particles, which is -1 if they overlap or 0 if they do not. The coefficients $E_{ll'}(q)$ are calculated via Monte Carlo integration techniques and are used in the expression for the Helmholtz free energy $\mathscr{F}_q[\psi]$ of a cholesteric phase that reads

$$\frac{\mathscr{F}_q[\psi]}{k_BTV} = n(\log n\mathscr{V} - 1) + 4\pi^2 n\int d\,\cos(\theta)\psi(\theta)\log\psi(\theta) + \frac{n^2G(\eta)}{2}\sum_{l,l'}\psi_l\psi_{l'}E_{ll'}(q), \tag{2}$$

where $n = N/V$ is the number density, N is the number of particles, V is the volume, T is the temperature, k_B is Boltzmann's constant, $\mathscr{V}$ is an (irrelevant) constant thermal volume, $G(\eta) = (1-0.75\eta)/(1-\eta)^2$ is the Parsons–Lee correction factor, and $\eta = nv_0$ is the packing fraction, with v_0 being the particle volume. Here, $\psi(\mathscr{R}) = \psi(\theta)$ is the orientation distribution function where only the dependence on the polar angle θ with respect to the local nematic director was kept, and ψ_l is the expansion coefficient. At fixed n, the free energy is minimized by iteratively solving the following equation:

$$\psi(\theta) = \frac{1}{Z}\exp\left\{-nG(\eta)\sum_{l,l'}\frac{E_{ll'}(q)}{4\pi^2}\frac{1}{2}[P_l(\cos\theta)\psi_{l'} + P_{l'}(\cos\theta)]\psi_l\right\}, \tag{3}$$

with Z being a normalization constant. This procedure is repeated for several values of the inverse pitch length q. Minimizing the free energy with respect to q gives the equilibrium pitch of the N^* phase.

The presented DFT is also generalized to binary mixtures to address the effect of size and shape polydispersity of CNCs on the phase behavior. The equilibrium pitch length of the N^* phase is again obtained by minimizing the free-energy functional, which for a binary mixture of two species $i = 1, 2$ has an additional mixing entropy term, an orientational free-energy term for each species, and both intra- and inter-species excluded volume terms, i.e.,

$$\frac{\mathscr{F}_q[\psi]}{k_B T V} = n(\log n\mathscr{V} - 1) + n\sum_{i=1}^{2} x_i \log x_i + 4\pi^2 n\sum_{i=1}^{2} x_i \int d\,\cos(\theta)\psi_i(\theta)\log\psi_i(\theta) + \frac{n^2 G(\eta)}{2}\sum_{i=1}^{2}\sum_{j=1}^{2} x_i x_j \sum_{l,l'} \psi_{il}\psi_{jl'} E^{ij}_{ll'}(q), \quad (4)$$

with $x_i = N_i/N$ being the number fraction of species i, N_i being the number of particles of species i, N being the total number of particles, $E^{ij}_{ll'}(q)$ being the excluded-volume coefficients between species i and j (intra-species for $i = j$ and inter-species otherwise) at cholesteric wave vector q, and ψ_{il} being the expansion coefficient of the orientation distribution $\psi_i(\theta)$ of species i.

The volume ratio of each species is defined as $\phi_i = x_i v_i/(x_1 v_1 + x_2 v_2)$, where v_i is the single particle volume of species i. It follows that $x_i = v_i^{-1}\phi_i/(v_1^{-1}\phi_1 + v_2^{-1}\phi_2)$.

B. Monte Carlo simulations

Monte Carlo (MC) simulations were employed in an orthorhombic simulation box with edges of length L_x, L_y, and L_z. In the case of periodic boundary conditions and since the cholesteric order is π-periodic, the simulation box imposes an intrinsic periodicity of wavelength $q_{L_z} = \pi/L_z$ as the system repeats itself in every periodic image. When the equilibrium state corresponds to a cholesteric phase with the chiral director along the z-axis and an inverse pitch length q that is not commensurate with an integer multiple of q_{L_z} (i.e., $\mathscr{P}/2 = L_z/k$, with k an integer), the system may become frustrated and equilibration may be hindered.

Various *ad hoc* methods have been developed to simulate the equilibrium properties of chiral nematic phases.[36,79–83] One simple but effective solution is to replace the periodic boundary conditions with boundary conditions that do not introduce an intrinsic periodicity of space.[39,84] In particular, under the assumption that the chiral director of the phase coincides with the z-axis, the periodic boundary conditions along the z-axis can be replaced by hard planar walls parallel to the xy-plane, thereby allowing for any periodicity of the cholesteric phase along the z direction. In this case, the system can freely relax to its equilibrium pitch length. The main drawback of this method is that the hard walls may affect the system's behavior in the proximity of the walls, and large system sizes may be needed to overcome wall effects.

MC simulations were performed on a system of $N = 4096$ CNCs modeled as chiral hard splinters consisting of N_c spherocylinders. Simulations were performed in the *NPT* ensemble, i.e., at fixed pressure P, temperature T, and the number of CNCs. Periodic boundary conditions were employed in the x- and y-directions and hard walls along the z direction. The overlap test between CNCs was performed by checking overlaps between the respective N_c hard spherocylinders.[85] To speed up the overlap test between the spherocylinders composing the CNCs, they were completely covered with a minimal mesh of overlapping spheres. Then, an overlap test between the meshing spheres was used as a pre-test: only overlaps between pairs of spherocylinders that have at least one overlapping meshing sphere were tested. This implementation of cell lists for the overlap between meshing spheres strongly reduces the computational cost of the overlap test between spherocylinders and thus also between CNCs.

The *NPT*-MC simulation scheme consists of two types of MC moves: roto-translation MC moves and volume-change moves. The first type of move consists of a random roto-translation of a randomly chosen CNC that is accepted if it does not lead to particle overlaps in the system, and otherwise, it is rejected. In a volume move, a random variation in the length of one of the three sides of the orthorhombic simulation box is proposed, resulting in either an expansion or compression of the system. If the move leads to overlaps, it is rejected; otherwise, it is accepted with a probability $P_{\text{acc}} = (V'/V)^N \exp(-\beta P(V' - V))$, where V and V' are the volume of the system before and after the move, respectively. During the simulation, we measure a variety of observables (density, uniaxial nematic order parameter, smectic order parameter, etc.).

Equilibration of the system is reached when all the sampled observables cease to drift and start to fluctuate around their mean value. The macroscopic pitch $\mathscr{P}$ of the cholesteric N^* phase was then measured. To this end, the simulation box was partitioned in slabs along the z-axis, and the nematic director $\hat{\mathbf{n}}(z_i)$ was measured in each slab, where z_i is the coordinate of the ith slab along the z-axis; a least-square fit of the theoretical expressions $n_x(z) = \cos(2\pi z/\mathscr{P} + \psi)$ and $n_y(z) = \sin(2\pi z/\mathscr{P} + \psi)$ for the x and y components of $\hat{\mathbf{n}}(z)$ yields a measure of the macroscopic pitch $\mathscr{P}$.

III. RESULTS AND DISCUSSION

A. The chiral hard-splinter model

Despite having a significantly irregular and polydisperse shape, widely dependent on the extraction method and the hydrolysis and/or sonication conditions,[6,41,42] a number of experimental observations suggest that cotton-based CNCs consist of slightly twisted bundles of laterally connected rod-like cellulose crystallites of well-defined cross section. This is confirmed (1) by observations using atomic force microscopy (AFM) and electron microscopy (EM)[43,44] or small angle scattering,[10,44] demonstrating that the total lengths and widths of the CNCs are described by broad log-normal distributions (lengths $L \approx 100$–200 nm and width $w \approx 15$–35 nm) but with a much better defined thickness (a Gaussian distribution centered around 6 ± 2 nm); and (2) by numerous observations of isolated microfibrils, revealing that the microfibrils are twisted,[16,43–46] and by atomistic simulations using various approaches, which all show independently that defect-free cellulose crystals spontaneously develop a gentle right-handed twist inversely proportional to the cross-sectional area.[40,47–52]

We, therefore, devise a simple hard-particle model, named the chiral hard-splinter (CHS) model, to account for the twisted splinter-like shape of cotton-based CNCs. A chiral hard splinter, sketched in Fig. 1, consists of N_c hard spherocylinders each modeling one of the crystallites composing the CNC. Each spherocylinder

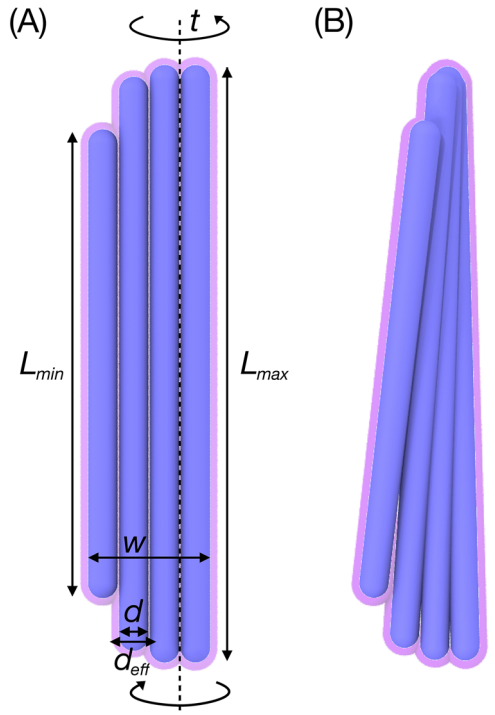

FIG. 1. Sketch of a generic chiral hard-splinter model. (a) The CNC is composed of N_c hard spherocylinders of diameter d and, here, an elliptical profile of lengths between two extreme values L_{min} and L_{max}, with total width w, and a shell of surfactant of thickness λ_S yielding an effective diameter $d_{eff} = d + 2\lambda_S$. Throughout this work, we, however, assumed $L = L_{min} = L_{max}$. (b) A twisted bundle of hard spherocylinders with a microscopic pitch length p obtained by applying a twist or rotation around a twist axis **t**, also called the screw axis. The motivation to choose this axis for the twist comes from molecular dynamics simulations,[40] showing that cellulose crystallites twist along this axis in a right-handed fashion.

i has a diameter d and a length L_i varying between $L_{min} \le L_i \le L_{max}$ following an elliptical profile. The center of the elliptical profile does not necessarily coincide with the central rod of the hard splinter. We note that L_i is the end-to-end length of spherocylinder i and thus includes the dimension of the hemispherical end caps. In addition, the spherocylinders twist with a microscopic pitch p around the twist axis **t**, also called the screw axis (see Fig. 1). To be more specific, we choose the twist axis parallel to the particle axes along the z-axis and denote the center of the twist axis by $(0, 0, 0)$. Points (x, y, z) in the bundle are rotated by an angle $\alpha = 2\pi z/p$. The motivation to choose this axis for the twist comes from molecular dynamics simulations,[40] showing that cellulose crystallites twist along this axis in a right-handed fashion. In order to take into account polydispersity in the width of the microfibrils, the total width w of a chiral hard splinter can be chosen to be smaller or larger than $N_c d$, allowing for some degree of overlap between the crystallites in the case the microfibrils are smaller in diameter or for having some gaps between the crystallites in the case the microfibrils are larger. In Fig. 2, we show that this particle model is sufficiently generic to capture the shape of various cotton-based CNCs as displayed by transmission electron microscopy (TEM) images. To illustrate how the shape of the hard splinter changes upon varying the various particle parameters, we refer the reader to the WebGL applet of the supplementary material.

B. The experimental system of cotton-based CNCs

To validate our chiral hard-splinter model with experimental data, we consider an experimental system of CNCs in an apolar solvent (e.g., toluene and cyclohexane), for which the self-assembly is largely driven by entropy. These suspensions may better elucidate the transfer mechanism of chirality from the molecular scale of the crystalline microfibrils to the self-assembly of CNCs into a cholesteric phase at the macroscopic scale. CNCs can be readily obtained from native cellulose sources via a harsh acid hydrolysis treatment.[53] Subsequently, the resulting CNCs can be sterically stabilized by surfactants in an apolar solvent, thereby fully masking the Van der Waals interactions, either by using surface functionalization or by using surfactants.[34,54–56] The latter way is much easier to implement and the resulting CNCs also self-assemble into cholesteric phases.[34] While in toluene the Van der Waals attractions are largely suppressed as the optical index of cellulose is nearly matched ($n_{cell} \approx 1.55 \pm 0.05$, $n_{tol} \approx 1.49$), some residual attractions may persist for CNCs in cyclohexane due to a small optical index mismatch ($n_{cyhex} \approx 1.43$). Furthermore, the low dielectric constants of these apolar solvents prevent the ionization of charges, which significantly reduces the electrostatic interactions. Consequently, the CNCs can be stabilized by adding surfactants that adsorb to the hydrophilic surface of the CNCs, and hence, CNCs suspended in apolar solvents with surfactants can be assumed to behave as nearly hard particles. The resulting excluded-volume interactions allow for much shorter distances between the CNCs, and hence, the CNC suspensions display cholesteric phases with much smaller pitches at much higher volume fractions, $\eta \approx 0.15$–0.35.

To allow for a quantitative comparison with experiments, we set the parameters of our model according to the geometry of the "Cot63" CNCs of Refs. 44 and 55. This "Cot63" sample was obtained via hydrolysis of cotton linters with 65% sulfuric acid at 63 °C for 30 min and was stabilized in cyclohexane using surfactants, ethoxylated phosphoric ester of nonylphenol (commercial name: BNA). This sample was chosen because of the high accuracy of the available data of this system on, for instance, the length, width, and thickness distributions of the CNCs and for the accurate measurements of the cholesteric pitch in bulk states of the chiral nematic phase. Measurements of the cholesteric pitch in the monophasic cholesteric regime instead of the biphasic regime is essential in order to avoid fractionation effects of the CNCs in the isotropic and cholesteric phase and to prevent a mismatch between the local volume fraction of the CNCs in the cholesteric phase and the average volume fraction across the two phases.

Although the CNCs of sample "Cot63" are highly polydisperse, the authors of Refs. 44 and 55 reported that the CNCs have a length $L = 128$ nm and width $w = 26$ nm with an additional 3 nm due to the surfactant layer contribution, i.e., 1.5 nm on each side. The dimension of a single crystallite is about 6.3 nm, which implies roughly four crystallites per CNC. Despite the large size and shape polydispersity of the "Cot63" sample, we model the bare CNCs as centrosymmetric chiral hard splinters, and each splinter consists of $N_c = 4$ spherocylinders with $L_{min} = L_{max} = L = 128$ nm, $w = 26$ nm, and $d = 6.3$ nm.

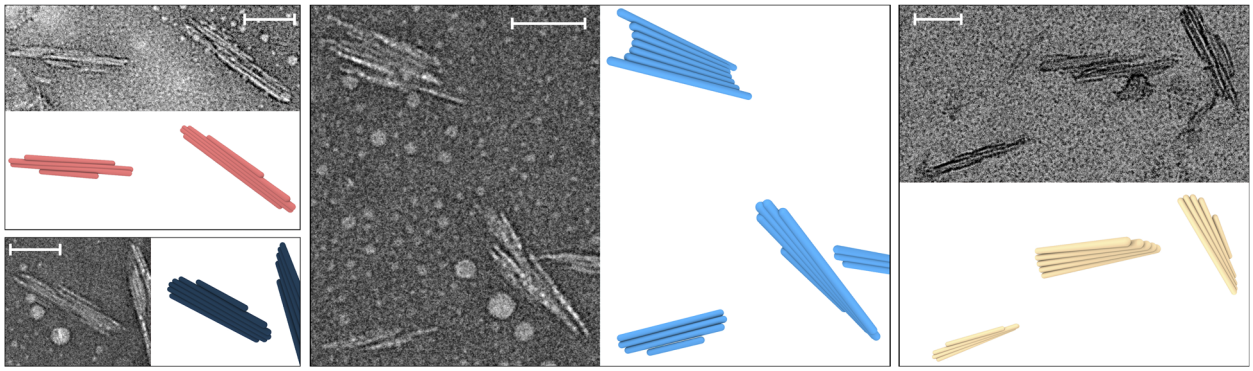

FIG. 2. Comparison of experimental observations of CNCs and their modeling using the model of chiral hard bundles. The variety of shapes seen in transmission electron microscopy (TEM) images of cotton-based CNCs (distinct from "Cot63" from Ref. 44) is modeled by the chiral hard-splinter model with a suitable choice of particle model parameters. Scale bars correspond to a 100 nm length.

The pitch length of the CNCs is harder to extrapolate from a two-dimensional electron microscope image. A precise experimental characterization of the microscopic twist of CNC crystallites is still lacking. The microscopic pitch was therefore estimated from all-atom molecular dynamics simulations of one single crystallite performed by Zhao *et al.*,[40] who reported a spontaneous right-handed twist of cellulose microfibrils with a microscopic pitch length linearly proportional to the inverse of its cross-sectional area. Assuming that the spontaneous twist of the CNCs is caused by the twist of its crystallites, we obtain a pitch length $p \sim 500$ nm for the whole splinter. We refer the interested reader to the supplementary material for more details how we estimated the microscopic pitch. To take into account the thickness of the surfactant layer, we use an effective diameter $d_{\text{eff}} = d + 2\lambda_S$ for the spherocylinders modeling the individual microfibrils of the CNCs in the chiral hard-splinter model, with $\lambda_S = 1.5$ nm being the thickness of the surfactant layer. The resulting chiral hard-splinter model for "Cot63" CNCs is shown in Fig. 3.

C. Monodisperse case

Employing our density functional theory (DFT) framework (see Sec. IV), we determine the isotropic I–cholesteric N^* phase transition for the "Cot63" CNCs, and subsequently, we predict the macroscopic pitch $\mathscr{P}$ of the N^* phase as a function of the effective packing fraction $\eta = nv_0(\lambda_S)$, where $n = N/V$ denotes the number density with N being the number of CNCs, V being the volume, and $v_0(\lambda_S)$ being the volume of a single CNC with a surfactant layer of thickness λ_S. We determine the volume of a single CNC $v_0(\lambda_S)$ via Monte Carlo simulations. To compare our theoretical predictions for the phase behavior as a function of the effective packing fraction η with experimental data, we convert the effective packing fraction in the w/w mass fraction. To this end, we first calculate the volume ratio of surfactants for a single CNC as $\phi_S = (v_0(\lambda_S) - v_0(\lambda_S = 0))/v_0(\lambda_S)$. In the case of a surfactant layer thickness $\lambda_S = 1.5$ nm, the surfactants constitute $\phi_S = 0.393$ of the particle volume. Employing the volume ratio of surfactant ϕ_S, we define an effective mass density of CNCs with adsorbed surfactants $\rho_{\text{eff}} = \rho_S\phi_S + \rho_{\text{CNC}}(1 - \phi_S)$, where ρ_S denotes the mass density of the surfactants and ρ_{CNC} denotes the mass density of the bare CNCs. We believe that this is a reasonable approximation, also employed in Ref. 54, due to the high density of the surfactant layer. Finally, the conversion of an effective packing fraction η into an effective w/w mass fraction reads $c_{\text{eff}} = \rho_{\text{eff}}\eta/(\rho_{\text{eff}}\eta + \rho_{\text{solv}}(1 - \eta))$, with ρ_{solv} being the solvent mass density.

In Fig. 3, we plot the macroscopic pitch length $\mathscr{P}$ of the predicted N^* phase of cotton-based CNCs as a function of the effective w/w mass fraction c_{eff} along with the experimental data. Our DFT calculations show that the cholesteric phase is stable with respect to the isotropic phase for a wide range of concentrations. The first thing

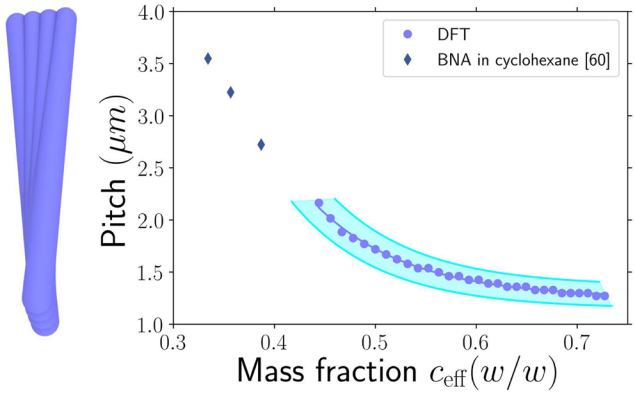

FIG. 3. Macroscopic pitch length $\mathscr{P}$ obtained from DFT calculations and from experimental observations in apolar CNC suspensions. The CNCs were modeled using the chiral hard-splinter model sketched on the left, with a surfactant layer of thickness $\lambda_S = 1.5$ nm, and reported in the corresponding mass fractions (violet circles) to compare directly with experimental observations (blue diamonds) made on cotton-based CNC suspensions stabilized in apolar solvents using surfactants (CNC@BNA in cyclohexane, data for "Cot63" from Ref. 55). Note that only experimental data from monophasic cholesteric phases are reported, and measurements in biphasic regions of the isotropic and cholesteric phase were excluded. The cyan band corresponds to a confidence region for variations of $2\lambda_S = 3\pm1$ nm in the DFT calculations. See Fig. S6 of the supplementary material for the macroscopic pitch as a function of volume fraction.

we can note is that, using DFT, a cholesteric phase is found above ~42%, while fully cholesteric CNC suspensions are experimentally observed already above ~32%. As discussed later, we ascribed this mismatch mostly to the monodispersity of the chiral bundles. The predicted cholesteric phase of "Cot63" CNCs is left-handed, implying that the macroscopic chirality has opposite handedness with respect to the microscopic chirality of the CNCs. Such a twist inversion is consistent with previous observations on systems of weakly chiral particles.[15,38,39] The macroscopic pitch $\mathscr{P}$ decreases monotonically with increasing concentrations, again in line with previous theoretical predictions.[15,38,39] However, this dependence does not follow a power law as predicted by Straley ($\mathscr{P} \sim \eta^{-2}$)[38] for chiral rigid rods or by Odijk ($\mathscr{P} \sim \eta^{-1}$)[57] for chiral semiflexible polymers. The discrepancy with Odijk's power law is to be expected as the CNCs are very rigid. Interestingly, extrapolating the DFT predictions to lower concentrations shows excellent quantitative agreement with the available experimental data. Previous studies have shown, however, that the DFT approach can only qualitatively predict trends of the cholesteric pitch as a function of particle details and thermodynamic state,[15] and this is also suggested by our comparison of DFT and MC simulations, as shown later in Sec. II F. Hence, we believe that the excellent agreement with the experimental data is fortuitous. In conclusion, our theoretical predictions for the cholesteric pitch $\mathscr{P}$ as a function of concentration, in qualitative agreement with the experiments with corresponding pitch values in the range of the experimental measurements, suggest that the cholesteric phase of CNCs is predominately driven by the shape of the cotton-based CNCs and that the cholesteric phase of CNCs in apolar solvents can be assumed to be entropy-driven as a first approximation.[58]

1. Effect of the microscopic pitch p

In our chiral hard-splinter model, the microscopic pitch p is the only parameter that could not be derived from experimental measurements on cotton-based CNCs but has been estimated from atomistic simulations.[40] We, therefore, investigate to what extent the microscopic pitch p affects the macroscopic pitch $\mathscr{P}$ of the cholesteric phase by repeating our DFT calculations for small variations of p while keeping the other particle model parameters fixed. The results are shown in Figs. 4 and S8. Interestingly, we find no significant change in the macroscopic pitch by changing the microscopic pitch p by up to 10%. Only at very high concentrations, $c_{\text{eff}} \gtrsim 0.6$, the macroscopic pitch is slightly affected by small variations in p. Thus, the agreement of our theoretical predictions on the macroscopic pitch with the experimental data persists, showing that our DFT results are robust with respect to small variations in the values of the microscopic pitch p.

2. Effect of the length and width of the CNCs

Subsequently, we investigate the effect of the dimensions of the bundles by simply varying the dimensions of the bundles in three different ways: (a) by varying the length of the CNCs independently of the width, "$(L\pm)$;" (b) by varying the width independently of the length, "$(w\pm)$;" and (c) by varying both the length and width, "$(\pm)$." We note that the thickness d is kept fixed in all three cases. For each specific shape, the exact shape of each particle, i.e., dimension, volume, and mass, is provided in the supplementary material.

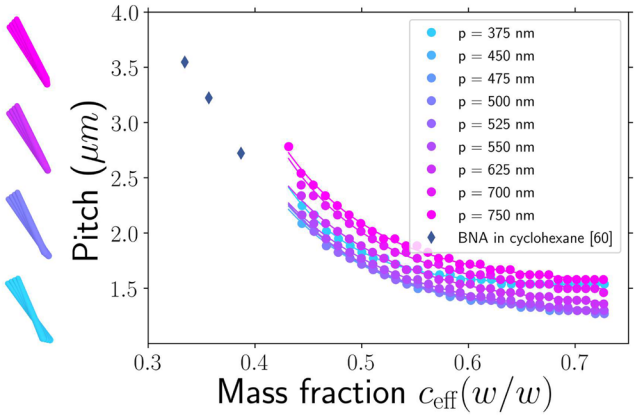

FIG. 4. Macroscopic pitch length $\mathscr{P}$ obtained from DFT calculations for varying values of the microscopic pitch p of the bundles and from experimental observations in apolar CNC suspensions. The CNCs were modeled using the chiral hard-splinter model with a surfactant layer of thickness $\lambda_S = 1.5$ nm. Experimental data are taken from cotton-based CNC suspensions stabilized in apolar solvents using surfactants (CNC@BNA in cyclohexane, data for "Cot63" from Ref. 55). Sketches of the chiral hard-splinter model for microscopic pitch lengths $p = 450$, 500 nm (taken as a reference), 550, and 700 nm (from bottom to top) are shown on the left. As a precise experimental characterization of the macroscopic twist on CNCs crystallites is still lacking at present, we estimated these values from atomistic simulations of CNCs, as from Refs. 40, where we assume that the twist in the bundle is equivalent to the twist on a single CNC. See Fig. S7 of the supplementary material for the macroscopic pitch as a function of volume fraction and Fig. S8 for the macroscopic pitch as a function of microscopic pitch.

a. The effect of the length L on $\mathscr{P}$. Using our DFT approach, we calculate the cholesteric pitch $\mathscr{P}$ for a monodisperse system of CNCs of length $L_{(\pm)} = L(1 + \delta)$, with δ being a scaling parameter. We present the cholesteric pitch $\mathscr{P}$ as a function of the effective w/w mass fraction in Fig. 5(a) for varying $\delta \in [-0.4, 0.4]$. We observe that the macroscopic pitch length $\mathscr{P}$ increases monotonically upon increasing the length L of the CNCs. This is in qualitative agreement with the theories of Straley and Odijk[38,57] and with simulations of chiral rods.[13,15] Shorter rods also require a higher mass fraction to stabilize the cholesteric phase, as expected from Onsager's theory for achiral spherocylinders.[19]

Revol *et al.* reported, in their seminal patent and associated publication (but unfortunately without any supporting data), that fractionation of CNCs into suspensions of shorter and longer CNCs impacts the cholesteric pitch according to Straley and Odijk, namely, that *longer* CNCs lead to *longer* pitches.[41,59] However, they specifically referred to the pitch measured in dried films once the suspension was dish-cast. Since then, this dependence has been taken for granted in the literature.[60,61] However, Honorato-Rios and Lagerwall recently reported, using fractionated aqueous CNC suspensions, that actually longer CNCs lead to smaller pitch values.[62] This result disagrees with the scenario of Fig. 5(a) and suggests that the change in pitch length is not only determined by the length of the CNCs.[62]

b. The effect of the width w on $\mathscr{P}$. Additionally, we determined the cholesteric pitch $\mathscr{P}$ for a monodisperse system of CNCs of width $w_{(\pm)} = w(1 + \delta)$. The results are presented in Fig. 5(b) for varying

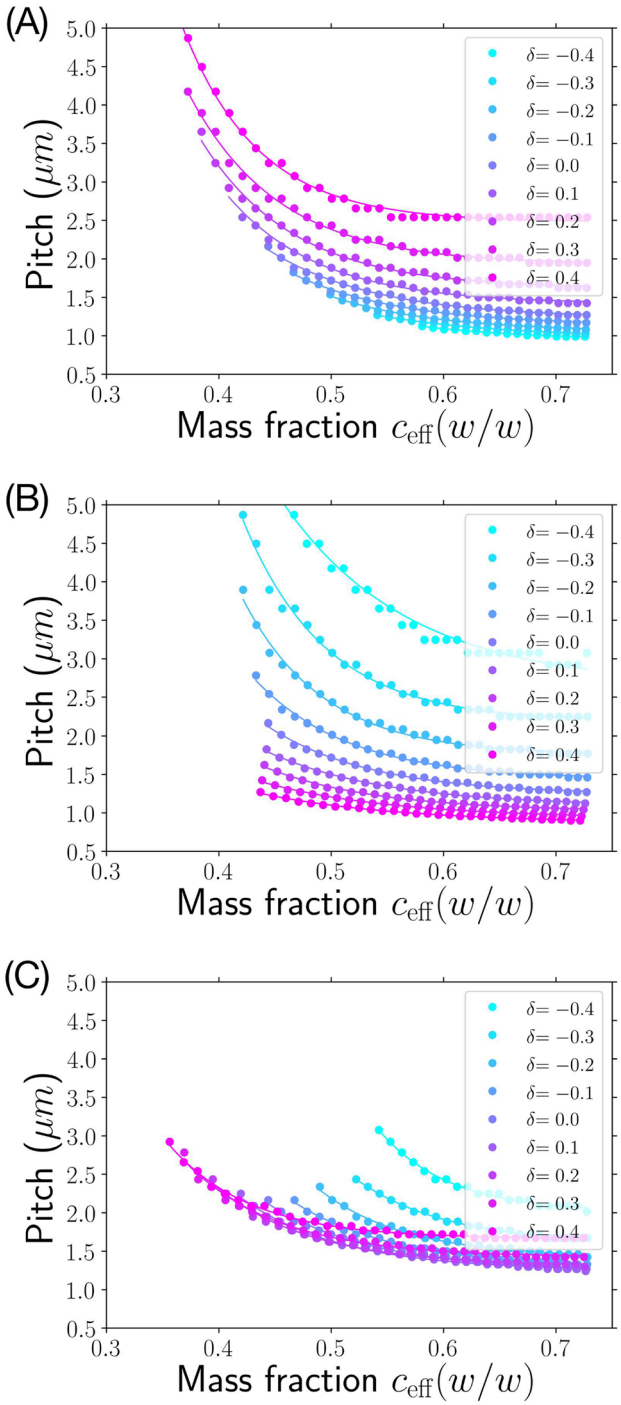

FIG. 5. Macroscopic pitch length $\mathscr{P}$ obtained from DFT for a cholesteric phase of monodisperse chiral hard splinters of different shapes. Effect of varying (a) the length $L_{(\pm)} = L(1+\delta)$ at fixed width w and thickness d, (b) the width $w_{(\pm)} = w(1+\delta)$ at fixed length L and thickness d, and (c) both the length $L_{(\pm)} = L(1+\delta)$ and the width $w_{(\pm)} = w(1+\delta)$ at fixed thickness d, for varying values of δ as labeled. Here, we set the reference length $L = 128$ nm and the width $w = 26$ nm before adding the surfactant contribution. See Fig. S9 of the supplementary material for the macroscopic pitch as a function of volume fraction.

$\delta \in [-0.4, 0.4]$. We find that the pitch length decreases monotonically upon increasing the width w of the CNCs, again in qualitative agreement with the theories of Straley and Odijk.[38,57] Importantly, the observed decrease in the pitch is much more pronounced even for moderate width variations. Odijk's description indeed predicts a scaling $\mathscr{P} \sim Ld(w-d)^{-1}$, qualitatively suggesting that a variation of the width w by a few nanometers, especially as it approaches the CNC thickness d, can have much stronger impact than a variation of L by a few tens of nanometers. This suggests that the relative variation of the width w may have a larger impact on the cholesteric pitch than for the length L of the CNCs.

To the best of our knowledge, we are not aware of any experimental study in the literature in which the effect of width w of the CNCs is investigated on the cholesteric pitch, while keeping the CNC length L fixed. As we will see, most size distribution analyses found that L and w are highly correlated.

c. Effect of both length L and width w on $\mathscr{P}$. Elazzouzi-Hafraoui *et al.* showed that the size distribution of CNCs exhibits strong correlation between L and w.[44] Moreover, recent fractionation experiments by Honorato-Rios *et al.* reported that the aspect ratios L/w of the CNCs in the two coexisting phases of large and small CNCs in biphasic suspensions are very similar, thereby also supporting a strong correlation between L and w.[63] As the cholesteric pitch $\mathscr{P}$ increases with increasing length L but decreases upon increasing the width w, it is interesting to investigate the effect of CNC size on the pitch, where both L and w vary and the aspect ratio L/w is kept constant.

We study the macroscopic pitch $\mathscr{P}$ for a monodisperse system of CNCs of length $L_{(\pm)} = L(1+\delta)$ and width $w_{(\pm)} = w(1+\delta)$ while keeping the aspect ratio L/w fixed. We plot the cholesteric pitch $\mathscr{P}$ as a function of the effective w/w mass fraction in Fig. 5(c) for varying $\delta \in [-0.4, 0.4]$. We observe that the macroscopic pitch $\mathscr{P}$ mostly decreases as the size, i.e., both L and w, increases from the smallest $\delta = -0.4$ to the largest dimension $\delta = 0.2$. This important observation shows that larger CNCs twist *more* than smaller CNCs. However, this observation seems to contradict the general and naive assumption that longer CNCs lead to longer pitches. CNCs that are larger in both their length and width rather have a stronger helical twisting power (HTP), and their presence in the suspension can act as "chiral dopants" similar to the chiral molecules added to achiral molecular nematic liquid crystals to induce cholesteric order.[64] This echoes with the recent work of Honorato-Rios and Lagerwall, where they even defined a Helical Twisting Power (HTP) associated with the CNCs and in first approximation proportional to the CNC size.[62] In their work, they consider the approximate relationship $1/\mathscr{P} = A(c_{\text{eff}} - c_0)$, where A is identified as the HTP and c_0 is a constant that they proposed to interpret as the threshold mass fraction required to convey chiral interactions. For comparison purposes, we reported $1/\mathscr{P}$ vs c_{eff} in Fig. S3 of the supplementary material, from which we extracted the parameters A and c_0 for different corresponding sizes $L_{(\pm)}$, which are reported in Fig. S4 of the supplementary material. We also plotted with a dashed line the approximate values of A and c_0 found by Honorato-Rios and Lagerwall.[62]

The behavior of sufficiently long rods, i.e., $\delta \geq 0.2$, is even more peculiar, as the macroscopic pitch $\mathscr{P}$ ceases to decrease further with size at low mass fractions but *increases* significantly at

high mass fractions. These two observations may be explained as follows. By decreasing δ and thus decreasing both L and w, the chiral hard splinter approaches the limit of a single achiral hard spherocylinder for which the macroscopic pitch $\mathscr{P}$ diverges, which hence explains the trend that $\mathscr{P}$ increases with decreasing size. This divergence as $w \to d$ is also captured by Odijk's scaling law as mentioned earlier. Likewise, as δ becomes larger, with L and w increasing proportionally, we expect from Odijk's scaling law an asymptotic stabilization of $\mathscr{P} \sim Rd(1 + d/w)$, where $R = L/w$ and d are both constant as δ increases. This behavior for large δ is also consistent with Straley's theory, which predicts a cholesteric pitch $\mathscr{P} = -2\pi K_2/K_T$ for weakly chiral particles, with K_2 being the twist elastic constant and K_T being the *chiral strength* of the cholesteric phase. In the case that the chiral strength K_T saturates at large enough δ and K_2 is expected to increase with δ, the macroscopic pitch $\mathscr{P}$ will increase upon increasing the particle dimension. This is indeed observed at high mass fractions, where the nematic order parameter S is expected to increase with c_{eff}, in qualitative agreement with Straley,[38] thereby rationalizing the non-monotonic variation of $\mathscr{P}$ with particle dimension at high c_{eff}. We note that the non-monotonic trend of the cholesteric pitch with concentration was also reported in Ref. 65, where the unwinding of the pitch at high concentrations was attributed by a strong increase in the local nematic order and a corresponding increase in the twist elastic constant K_2.

D. Bidisperse case of large and small CNCs

We have shown that in the case of a monodisperse suspension, the size of the CNCs influences the cholesteric pitch $\mathscr{P}$ and that larger chiral splinters, when scaled up both in length and width, lead to a *stronger* chiral behavior and hence a smaller pitch $\mathscr{P}$. Experimental suspensions of CNCs are usually characterized by a highly polydisperse log-normal size distribution of CNCs, which may affect the cholesteric pitch $\mathscr{P}$. However, our DFT approach cannot straightforwardly be extended to take into account a log-normal size distribution. We, therefore, model the polydispersity by considering a mixture of a number of distinct components similar to Ref. 66. As the computational cost increases rapidly with the number of components, we study the cholesteric pitch for bidisperse suspensions of large and small CNCs in order to shed some light on the effect of size polydispersity of the CNCs on the macroscopic pitch $\mathscr{P}$.

1. Size distribution of "Cot63" as a starting point

CNC suspensions are usually characterized by transmission electron microscopy (TEM) or AFM, allowing for measurements of the size distributions, the averaged dimensions $(\bar{L}, \bar{w})$ and the corresponding standard deviations, σ_L and σ_w, and covariance, $\text{cov}(L, w)$. For "Cot63," the average dimensions were reported ($\bar{L}$ = 126 nm and $\bar{w}$ = 26 nm) as well as their respective standard deviations $\sigma_L \approx 71$ nm and $\sigma_w \approx 8.3$ nm. Unfortunately, Elazzouzi-Hafraoui *et al.* did not provide a bivariate size distribution analysis in their study on the "Cot63" sample, but they provided a fit of the two-dimensional size distributions for two other samples, "Cot45" and "Cot72," prepared at slightly lower and higher temperatures, 45 and 72 °C, respectively. In both cases, they observed strong correlation between L and w defined as $\text{corr}(L, w) = \text{cov}(L, w)/(\sigma_L \sigma_w)$, which were given by $\text{corr}(L, w) \approx 0.74$ and $\text{corr}(L, w) \approx 0.66$, as obtained by fitting the respective bivariate distributions, and both follow a roughly proportional relationship ($L \sim w$). As a comparison, the correlation between L/w and L for the two samples were found to be $\text{corr}(L/w, L) \approx 0.01$ and 0.41, respectively.

In order to investigate how the cholesteric pitch $\mathscr{P}$ is affected by polydispersity, we consider a bidisperse suspension of large and small CNCs denoted by (+) and (−), respectively, and we define the respective shapes of the CNCs with respect to the reference dimensions of "Cot63." This bidisperse mixture is characterized by the parameter δ as introduced above. We denote the number fraction of large CNCs (+) in the mixture by $x_{(+)}$, while the fraction of smaller CNCs (−) is defined as $x_{(-)} = 1 - x_{(+)}$. From the data available on "Cot45" and "Cot72," we expect that about 55%–65% of the CNCs fall within the sizes defined by $\delta = \pm 0.4$. Alternatively, the bidisperse suspension of CNCs can be defined for a given volume ratio $\phi_{(+)}$ instead of the number fraction $x_{(+)}$. This is particularly relevant when large and small particles are mixed together at equal concentration, since the relative mixture of the two samples directly reflects the volume ratio $\phi_{(+)}$ in the final mixture rather than $x_{(+)}$.

2. Effect of size difference via δ

We consider a bidisperse suspension of large (+) and small (−) CNCs at a fixed number fraction $x_{(+)} = 0.5$. We calculate the cholesteric pitch $\mathscr{P}$ as a function of the effective mass fraction c_{eff} for varying values of δ and show the results in Fig. 6(a). We observe that the mass fraction at which the cholesteric phase forms decreases with increasing δ, i.e., for increasing size difference between the large and small CNCs, thereby bringing the transition to the cholesteric phase closer to the experimental observations. It is also important to note here that we did not consider the possibility of fractionation, which has been considered in Ref. 67. However, we remark that the experimental measurements were performed in the monophasic cholesteric regime instead of the biphasic regime in order to avoid fractionation effects. At a sufficiently high mass fraction, the macroscopic pitch $\mathscr{P}$ also becomes larger upon increasing δ, but this mass fraction regime is probably experimentally irrelevant as the CNC suspensions are most likely kinetically arrested. However, if we keep the volume ratio $\phi_{(+)} = 0.5$ fixed, we observe from Fig. 6(b) an overall shift to larger pitches, which may be explained by the higher number of small particles of weaker helical twisting power in comparison to the number of large particles. We note that the increase in the macroscopic pitch with increasing polydispersity is consistent with previous work, where it was shown that the macroscopic twist of a cholesteric phase can be reduced by increasing the length polydispersity of a nanorod suspension.[67]

3. Effect of composition via $\phi_{(+)}$

We now consider bidisperse suspensions of large and small CNCs defined at a fixed δ and varying volume ratios $\phi_{(+)}$ of large CNCs ranging from 0 to 1. We calculate the cholesteric pitch $\mathscr{P}$ as a function of the effective mass fraction c_{eff} and show the results in Fig. 7 for $\delta = 0.1$ and $\delta = 0.4$. Other values of δ are reported in the supplementary material (Fig. S2), and the corresponding $x_{(+)}$ values are listed in Table S2. We clearly observe from Fig. 7 a gradual transition from a monodisperse population of small CNCs ($\phi_{(+)} = x_{(+)} = 0$) to a monodisperse population of large CNCs

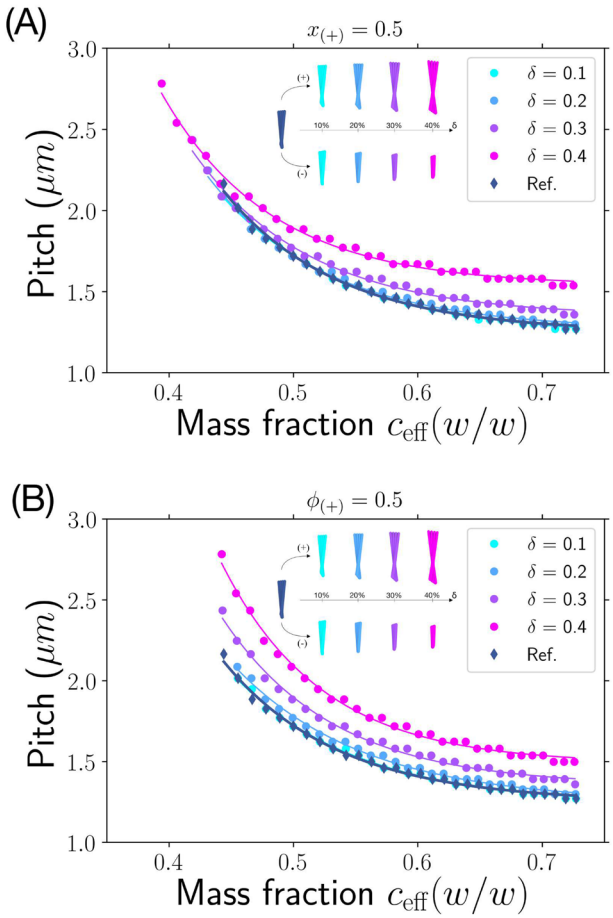

FIG. 6. Macroscopic pitch length $\mathscr{P}$ obtained from DFT for a cholesteric phase of bidisperse chiral hard splinters of various sizes and fixed L/w aspect ratio. (a) The large and the small particles have an equal number fraction ($x_{(+)} = x_{(-)} = 1/2$) or (b) equal volume ratio ($\phi_{(+)} = \phi_{(-)} = 1/2$). The dimensions [$L_{(\pm)} = L(1 \pm \delta)$ and $w_{(\pm)} = w(1 \pm \delta)$] are scaled as a function of δ. The monodisperse case ($\delta = 0$, denoted as Ref.) is displayed for reference. See Fig. S10 of the supplementary material for the macroscopic pitch as a function of volume fraction.

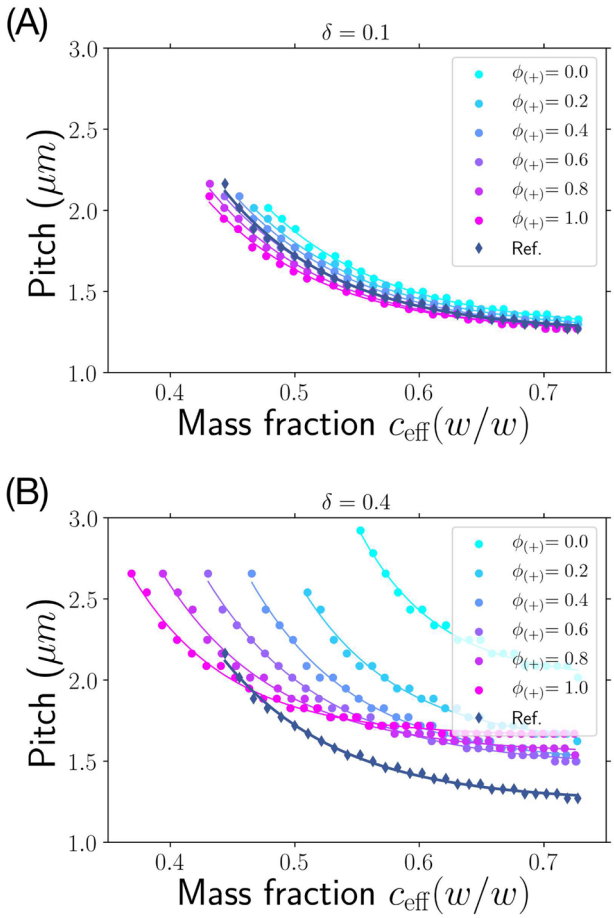

FIG. 7. Macroscopic pitch length $\mathscr{P}$ obtained from DFT for a cholesteric phase of bidisperse chiral hard splinters of large and small particles of fixed L/w aspect ratio and various volume ratios $\phi_{(+)}$ of large particles. The effect of the dimensions of the large and the small particles is defined by [$L_{(\pm)} = L(1 \pm \delta)$ and $w_{(\pm)} = w(1 \pm \delta)$] with (a) $\delta = 0.1$ and (b) $\delta = 0.4$ (for intermediate values of δ, see the supplementary material). The monodisperse case ($\delta = 0$, denoted as Ref.) is displayed for reference. See Fig. S11 of the supplementary material for the macroscopic pitch as a function of volume fraction.

($\phi_{(+)} = x_{(+)} = 1$), where we retrieve the conclusions from the monodisperse case discussed before, i.e., the cholesteric pitch $\mathscr{P}$ decreases with increasing size of the CNCs.

For intermediate volume ratios where the system is bidisperse, we observe a monotonic decrease in the cholesteric pitch $\mathscr{P}$ for increasing $\phi_{(+)}$ for an effective mass fraction ($c_{\text{eff}} \leq 55$ wt. %), showing that the macroscopic pitch results from a trade-off between large CNCs, favoring small pitches, and small CNCs, favoring large pitches. A non-monotonic behavior of the cholesteric pitch with $\phi_{(+)}$ is found at high mass fractions and high δ, possibly due to a stronger twisting power between small and large CNCs, e.g., a small CNC may fit inside a chiral "groove" of a larger one. However, these high effective mass fractions may be inaccessible experimentally due to kinetic constraints, which we speculate to occur at about ≥45 wt. %.

In Fig. 7, we plot the macroscopic pitch $\mathscr{P}$ for equally spaced values of $\phi_{(+)}$ instead of $x_{(+)}$ in order to compare with experimental findings, which will be discussed in Sec. II E. This choice becomes more significant at high δ, where the particle volumes of the large and small CNCs start to deviate more, and consequently, also the difference between $x_{(+)}$ and $\phi_{(+)}$, e.g., in Fig. 7(b) for $\delta = 0.4$, $\phi_{(+)} \approx 0.8$, corresponds to $x_{(+)} \approx 0.5$.

Experimentally, the size polydispersity is defined by a size distribution in terms of number fractions. In order to estimate the effect of bidispersity, one should compare the cholesteric pitch at $x_{(+)} \approx 0.5$, i.e., $\phi_{(+)} \approx 0.8$ with the reference (Ref.) curve. We find that for the bidisperse case, the cholesteric phase is stable at lower effective mass fractions than in the monodisperse reference system. Additionally, we find that the macroscopic pitch for the bidisperse

system at $\phi_{(+)} \approx 0.8$ is lower than for the monodisperse system at low mass fractions, but higher for mass fractions above 45 wt. %. Another interesting observation is that above $\phi_{(+)} \approx 0.8$, the pitch values do not change much until $\phi_{(+)} \approx 1$. This suggests that the twisting power of the larger CNCs saturates when $x_{(+)} > 0.5$, which could be inherent to their finite microscopic pitch p. The fact that the short CNCs do not display a similar saturation supports this interpretation.

E. Comparison with experimental observations

1. Implications for size fractionation of CNCs

As mentioned earlier, one can gradually enrich or deplete certain CNC subpopulations by exploiting the effect of fractionation in biphasic samples. This has been successfully implemented by Revol, Dong, and co-workers and more recently reproduced by Honorato-Rios *et al.* to produce suspensions with enriched proportions of larger or smaller CNCs, whereby the larger rods were accumulated in the anisotropic phase and the shorter ones in the isotropic state.[41,59,62,63,68,69]

There are not many experimental observations of the pitch variation with size fractionation in suspension and all we found were done in aqueous suspensions. Until recently, only indirect clues of this effect were available in the literature, namely, (a) spatial variations of the pitch in sealed capillaries in the biphasic regime, with smaller pitches at the bottom and larger pitches near the interface between the two phases (see Ref. 70, Fig. S16); and (b) pitch differences observed across cast film thicknesses, reported by Klockars *et al.*[69] or Zhu *et al.*[71] The most spectacular evidence of this effect was presented recently by Honorato-Rios and Lagerwall, where the pitch was studied in suspensions of fractionated CNCs, and it was found to be inversely proportional to the average CNC length L.[62] The authors also reported a correlation between L and w, validating this comparison. However, quantitative comparison with the data reported by these authors is difficult, as the range of the mass fraction is very different in water and in apolar solvents. The estimated HTP they reported lays within the same range of values as those we reported in Fig. S4, but the constant c_0 appears to be much smaller than what we found.

2. Implications for tip sonication treatments of CNCs

A second strong experimental validation of this chiral hard-splinter model is the observation reported by Beck *et al.* that the application of a tip sonication treatment leads to an increase in the cholesteric pitch $\mathscr{P}_{\text{film}}$ observed both in suspensions and in films produced by dish-casting CNC suspensions.[60] We note that these authors used another source of CNCs, made from bleached softwood kraft pulp by FPInnovation, but since then, they have confirmed their observations on many other sources of CNCs, including cotton.

While most of their work discusses the effect of sonication on the cholesteric pitch $\mathscr{P}_{\text{film}}$ of solid films, they also show an increase in the macroscopic pitch $\mathscr{P}$ of the cholesteric phase in a suspension at 5 wt. % along with a decrease in volume fraction of the cholesteric phase.

To understand this observation, it is important to consider that tip sonication, which is routinely used to improve the dispersion of CNCs in various solvents, makes the suspensions visibly less turbid, an effect that can be associated with the break-up of the largest CNCs into smaller ones.[68] This observation has been quantitatively observed by Csiszar *et al.*[72] They reported from their TEM analysis that tip sonication decreases the dimensions of cotton-sourced CNCs, from $\bar{L} = 171 \pm 57$ nm and $\bar{w} = 17 \pm 4$ nm after only 1 min to $\bar{L} = 118 \pm 45$ nm and $\bar{w} = 13 \pm 3$ nm after 10 min.[72] This suggests an approximately linear dependence between $\bar{L}$ and $\bar{w}$, in agreement with our assumption. Using a different source of wood pulp derived CNCs (UMaine Development Centre, Forest Product Laboratory, USA), Gicquel *et al.* reported an even more important lateral break-up of CNCs, reporting a length decrease from $\bar{L} = 217 \pm 42$ nm to $\bar{L} = 150 \pm 30$ nm after tip sonication (from AFM and TEM analyses) and a width decrease from $\bar{w} \approx 60$ nm to $\bar{w} \approx 20$ nm after tip sonication (from SAXS analysis), while the CNC thickness $d \approx 4$–5 nm (from AFM analysis) remained relatively unaffected.[73] A decrease in both L and w appears to be a generic consequence of tip sonication in CNC suspensions and validates our size scaling predictions on the cholesteric pitch of sonicated samples.

However, in Ref. 60, Beck *et al.* excluded in their work the breakdown of CNCs into shorter rods as a possible explanation for the pitch variation, as they assumed that shorter rods would *decrease* the pitch, thereby referring to Revol *et al.*[41] The authors also mentioned, citing Ref. 68, that tip sonication breaks the CNCs side-by-side, and therefore, it should decrease the average width w, assuming that both smaller L and w would lead to smaller $\mathscr{P}$, in contrast to what is predicted by our model [see Fig. 5(c)]. They also reported an increase in the mass fraction at which the cholesteric phase appears. They did monitor the CNC size only via dynamic light scattering (DLS) but did not notice an obvious change of hydrodynamic diameters between samples (data not provided). Finally, as size exclusion chromatography coupled with multi-angle laser light scattering (SEC-MALLS) showed that the weight-average degree of polymerization (DP = 140–150) of the cellulose chains within their CNCs was unaffected by the sonication energy applied in their experiments, they proposed that the pitch increase was due to a release of trapped ions, since they also noticed an increase in conductivity. However, this scenario, which has also been criticized on the ground of rheological studies (cf. Ref. 74), appears somewhat inconsistent, since the release of these ions, and hence a higher ionic strength, is primarily known to *decrease* $\mathscr{P}$ in suspensions and in resulting dish-cast films.[41]

The proposed chiral hard-splinter model here offers a much more convincing and simpler explanation: Tip sonication breaks the larger CNCs into smaller CNCs and effectively decreases $\phi_{(+)}$. As the large CNCs contribute the most to the twisting, their destruction unwinds the cholesteric phase and increases the pitch. It also accounts for the increase in the mass fraction at which the cholesteric phase appears, as shown in Fig. 5. The moderate increase in conductivity that was reported for their sample can be explained by the release of trapped ions as suggested by the authors or by an increase in the total surface area of the CNCs due to the splitting of the bundles, which not only decreases the surface charge per CNC but also reduces the number of counter-ions in the Stern layers. As a consequence, extra ions are released from the surface of the CNCs, which increases the ionic strength. The lower surface charge per CNC as well as the higher ionic strength will lead to weaker repulsions between the CNCs, which is the opposite of what was proposed by the authors. The splitting of bundles into smaller bundles,

without breaking the microfibrils, also accounts for the unaffected DP of the cellulose chains they reported. While our simple scaling model for both the length and width of the CNCs suggests that longer bundles require longer crystalline subunits, we can also refer to Figs. S1 and S2 of the supplementary material to convince ourselves that the average length of the constituents of a bundle is necessarily smaller than the length of the bundle itself.

F. Validation of the theoretical predictions with MC simulations

Our theoretical framework is based on a second-virial approximation and ignores higher-order correlations, which may become important at higher packing fractions. In addition, the theory assumes local uniaxial order, whereas biaxial order is expected to be strongly coupled to chiral order.[29,75] Our theoretical approach has been tested against simulations of hard twisted triangular prisms, showing that the handedness of twist, order of magnitude of the cholesteric pitch, and the trends of the macroscopic chiral behavior as a function of particle shape and thermodynamic state are well predicted by our DFT calculations.[15] Here, we test our theoretical predictions against MC simulations on a monodisperse system of hard splinters. We perform both DFT calculations and MC simulations on a system of centro-symmetric (i.e., with twist axis **t** matching the particle axis) chiral hard splinters of slightly different dimensions, composed of $N_c = 4$ spherocylinders, with $L_{min} = L_{max} = 100$ nm, $w = 20$ nm, $d = 8.0$ nm, and no surfactant layer ($\lambda_S = 0$ and $d_{eff} = d$). In this case, DFT calculations predict a wide region of stability of the left-handed cholesteric phase, which is confirmed in the MC simulations (see Fig. 8). In particular, we plot the macroscopic pitch length $\mathscr{P}$ as a function of packing fraction η as measured in MC simulations along with the DFT predictions in Fig. 9. We find that although the theory predicts smaller pitch lengths $\mathscr{P}$ than the ones found in simulations, the pitch length of the cholesteric phase obtained from MC simulations compares reasonably well with the experimental pitch lengths and shows the same decreasing trend with η. We also show a typical configuration of the cholesteric phase of the simulated chiral hard-splinter model at packing fraction $\eta = 0.47$.

We make the following observations. First, our DFT predictions for the macroscopic pitch length compare well with the available experimental data on the pitch lengths for monodisperse suspensions of "Cot63" CNCs in apolar solvents. On the one hand, we find that bidispersity decreases the pitch length and decreases the mass fraction of the stability region of the cholesteric phase. On the other hand, we find that MC simulations on slightly different hard splinter dimensions show that the pitch length should actually be larger than the DFT predictions. Assuming that these effects on $\mathscr{P}$ are robust with respect to slight variations of the shape parameters of the hard splinter model, they would seem to compensate each other. Additionally, the mass fraction at which the cholesteric phase is predicted to be stable from DFT calculations is much higher than observed in experiments but bidispersity shifts the stability regime of the cholesteric phase to lower mass fractions. Moreover, while the van der Waals interactions are nearly vanishing for CNCs in toluene due to an almost perfectly matching optical index, the CNC suspension considered here is dispersed in cyclohexane, and hence, the dispersion (van der Waals) forces are not fully masked as a result of a small mismatch in the optical index. As a consequence, the interaction potentials between the CNCs are not simply excluded-volume interactions, but residual short-range attractions are exerted between the CNCs, which will also shift the stability region of the cholesteric phase to lower mass fractions and thus closer to the experimental values. In addition, the residual attractions also

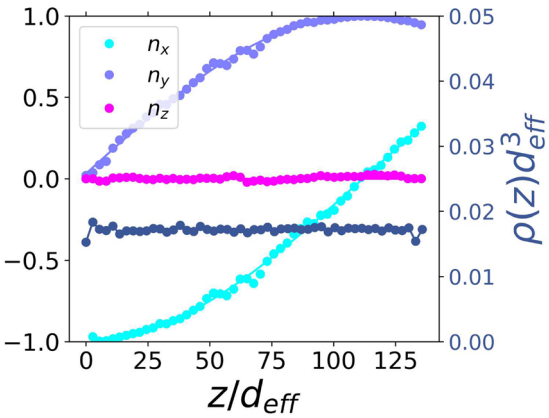

FIG. 8. Observation of a cholesteric order in Monte Carlo simulations using the chiral hard-splinter model. The shape of the particles was chosen to correspond to cotton-based "Cot63" CNCs suspended in a apolar solvent with a surfactant layer of thickness $\lambda_S = 1.5$ nm at packing fraction $\eta = 0.47$. The x, y, and z components of the nematic director field $\hat{\mathbf{n}}(z) = (n_x(z), n_y(z), n_z(z))$ as a function of z. The color-matching lines correspond to a fit of the theoretical nematic director field $\hat{\mathbf{n}}(z) = (\cos(2\pi z/\mathscr{P} + \psi), \sin(2\pi z/\mathscr{P} + \psi), 0)$, which yield a measure of the macroscopic pitch $\mathscr{P}$ (see Fig. 9). The blue points correspond to the local number density $n(z)d_{eff}^3$ as a function of z, showing that the effect of the hard walls on the bulk of the simulation box is negligible.

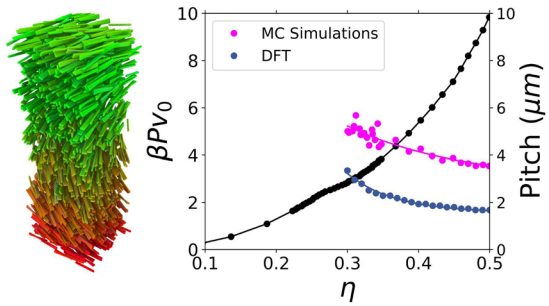

FIG. 9. Macroscopic pitch length $\mathscr{P}$ obtained from Monte Carlo simulations and from DFT calculations for the cholesteric phase of monodisperse chiral hard splinters. For this comparison, we used a monodisperse system of chiral hard splinters with $N_c = 4$ spherocylinders, $L_{min} = L_{max} = 100$ nm, $w = 20$ nm, $d = 8.0$ nm, and $\lambda_S = 0$ and reported the pitch for Monte Carlo (MC) simulations (magenta circles) and DFT calculations (blue circles) as a function of the (volumetric) packing fraction η. The black line denotes the equation of state $\beta P v_0$ vs η. The comparison is reasonable within the expected quantitative errors of the DFT calculations. MC simulations confirm that our simple hard-particle model of CNCs stabilizes a cholesteric phase with a macroscopic pitch length in reasonable agreement with experimental values. A typical simulation configuration of the left-handed cholesteric phase at $\eta = 0.47$ is shown on the left, with particles colored according to their orientation.

explain the experimental observation of a kinetically arrested gel at sufficiently high mass fractions, roughly above 45 wt. %. Including the attractive interactions in our MC simulations will increase the twisting power between the CNCs, and the simulated values for the cholesteric pitch $\mathscr{P}$ will decrease and become closer to the experimental values. In addition, it is indeed known that a higher ionic strength allows for closer interactions between the CNCs, thereby enhancing the twisting power and reducing the cholesteric pitch.[76]

IV. CONCLUSIONS

We developed a simple hard-particle model, the chiral hard-splinter model, to describe the behavior of cotton-based CNCs assemblies in apolar solvents with surfactants. To test this model, we chose the particle model parameters such that the shape matches the typical shape of cotton-based "Cot63" CNCs from Refs. 44 and 55. A chiral hard splinter consists of a chiral bundle of N_c hard spherocylinders, each modeling one of the crystalline microfibrils composing the CNC. The layer of surfactants adsorbed to the CNCs is modeled by using an effective diameter of the crystallites composing the CNCs. We accounted for the density of the CNCs and surfactant to compare our simulation to actual pitch measurements expressed in mass fractions.

We employed a recently developed DFT approach to study the cholesteric phase of our model system. We test the validity of our theoretical calculations against MC simulations. Importantly, we observed that our simple hard-particle model of right-handed CNCs stabilizes a left-handed cholesteric phase (i.e., an inversion of chirality) with macroscopic pitch values $\mathscr{P}$ that compare well with the experimental findings. This model predicts that $\mathscr{P}$ *decreases* with the size of the CNCs, which is contrary to current beliefs and supports most recent experimental observations on the effect of fractionation on the macroscopic pitch[62] but also the redshift induced by tip sonication.[60] Moreover, our theoretical predictions for the cholesteric pitch lengths using this hard-splinter model are in good agreement with the experimental observations for CNC suspensions in apolar solvents, primarily relevant for this work.

In general, our findings suggest that the clustering of cellulose crystallites into chiral twisted bundles, which constitute the CNCs, is the missing link explaining the highly debated chirality transfer mechanism in the nanocellulose community, from the molecular level (the D-glucose monomers) and the twisted crystallites to the formation of a cholesteric liquid crystal phase in suspension. The chiral shapes of the CNCs are *sufficient* to induce a purely entropy-stabilized cholesteric phase with a pitch length in good agreement with the experimentally measured ones. Monte Carlo simulations show that the pitch length should be larger than the predictions from the DFT calculations, whereas polydispersity increases the pitch length. Other effects such as residual (chiral) van der Waals (including dipolar[56]) interactions may decrease the pitch as well.[77]

While the chiral hard-splinter model allows us to capture most of the experimental observations on the chiral behavior of CNCs in concentrated suspensions, a refinement based on an analogous chiral soft-splinter model may account for the residual (van der Waals) interactions of CNCs in apolar solvents but also for strong electrostatic repulsions in the case of aqueous CNC suspensions.[15] While first attempts have recently been made to demonstrate the presence of bundles and their impact on the self-assembly in CNC water suspensions,[78] we hope that our work will further inspire experimental investigations on the cholesteric pitch of well-characterized CNCs in both apolar as well as aqueous suspensions to fully validate the chiral hard-splinter model.

SUPPLEMENTARY MATERIAL

See the supplementary material for the WebGL applet for the chiral hard-splinter model, the dimension characteristics of the model of CNC bundles employed, the volume to mass fraction conversion factors (monodisperse and bidisperse cases), additional DFT curves for the bidisperse case, and all DFT curves expressed vs the packing fraction η.

ACKNOWLEDGMENTS

The authors acknowledge Thomas Parton for providing TEM images of CNC bundles. This work was supported by the European Union's Horizon 2020 Research and Innovation Programme (Grant Agreement No. 676045), a BBSRC David Phillips fellowship (Grant No. BB/K014617/1), the EPSRC (Grant Nos. EP/K503757/1 and EP/R511675/1), the European Research Council (Grant No. ERC-2014-STG H2020 639088), and ERC-2019-ADV-H2020 884902.

AUTHOR DECLARATIONS

Conflict of Interest

The authors have no conflicts to disclose.

DATA AVAILABILITY

The data that support the findings of this study are openly available from the University of Cambridge data repository at http://doi.org/10.17863/CAM.53675 (reference number 1203141).

REFERENCES

[1] E. Kontturi, P. Laaksonen, M. B. Linder, A. H. Nonappa, A. H. Gröschel, O. J. Rojas, and O. Ikkala, "Advanced materials through assembly of nanocelluloses," Adv. Mater. **30**, 1703779 (2018).
[2] J. R. Barnett and V. A. Bonham, "Cellulose microfibril angle in the cell wall of wood fibres," Biol. Rev. **79**, 461–472 (2004).
[3] D. J. Cosgrove and M. C. Jarvis, "Comparative structure and biomechanics of plant primary and secondary cell walls," Front. Plant Sci. **3**, 204 (2012).
[4] D. R. Smyth, "Helical growth in plant organs: Mechanisms and significance," Development **143**, 3272–3282 (2016).
[5] B. D. Wilts, H. M. Whitney, B. J. Glover, U. Steiner, and S. Vignolini, "Natural helicoidal structures: Morphology, self-assembly and optical properties," Mater. Today: Proc. **1**, 177–185 (2014).
[6] J.-F. Revol, H. Bradford, J. Giasson, R. H. Marchessault, and D. G. Gray, "Helicoidal self-ordering of cellulose microfibrils in aqueous suspension," Int. J. Biol. Macromol. **14**, 170–172 (1992).
[7] M. Mitov, "Cholesteric liquid crystals in living matter," Soft Matter **13**, 4176–4209 (2017).

[8]B. Frka-Petesic and S. Vignolini, "So much more than paper," Nat. Photonics **13**, 365–367 (2019).
[9]Y. Ogawa, "Release of internal molecular torque results in twists of glaucocystis cellulose nanofibers," Carbohydr. Polym. **251**, 117102 (2021).
[10]A. N. Fernandes, L. H. Thomas, C. M. Altaner, P. Callow, V. T. Forsyth, D. C. Apperley, C. J. Kennedy, and M. C. Jarvis, "Nanostructure of cellulose microfibrils in spruce wood," Proc. Natl. Acad. Sci. U. S. A. **108**, E1195–E1203 (2011).
[11]J. P. F. Lagerwall, C. Schütz, M. Salajkova, J. Noh, J. Hyun Park, G. Scalia, and L. Bergström, "Cellulose nanocrystal-based materials: From liquid crystal self-assembly and glass formation to multifunctional thin films," NPG Asia Mater. **6**, e80 (2014).
[12]C. De Michele, L. Rovigatti, T. Bellini, and F. Sciortino, "Self-assembly of short DNA duplexes: From a coarse-grained model to experiments through a theoretical link," Soft Matter **8**, 8388 (2012).
[13]H. B. Kolli, E. Frezza, G. Cinacchi, A. Ferrarini, A. Giacometti, T. S. Hudson, C. De Michele, and F. Sciortino, "Self-assembly of hard helices: A rich and unconventional polymorphism," Soft Matter **10**, 8171–8187 (2014).
[14]S. Belli, S. Dussi, M. Dijkstra, and R. van Roij, "Density functional theory for chiral nematic liquid crystals," Phys. Rev. E **90**, 020503 (2014).
[15]S. Dussi, S. Belli, R. van Roij, and M. Dijkstra, "Cholesterics of colloidal helices: Predicting the macroscopic pitch from the particle shape and thermodynamic state," J. Chem. Phys. **142**, 074905 (2015).
[16]Y. Ogawa, "Electron microdiffraction reveals the nanoscale twist geometry of cellulose nanocrystals," Nanoscale **11**, 21767–21774 (2019).
[17]J. Majoinen, J. S. Haataja, D. Appelhans, A. Lederer, A. Olszewska, J. Seitsonen, V. Aseyev, E. Kontturi, H. Rosilo, M. Österberg, N. Houbenov, and O. Ikkala, "Supracolloidal multivalent interactions and wrapping of dendronized glycopolymers on native cellulose nanocrystals," J. Am. Chem. Soc. **136**, 866–869 (2014).
[18]M. Kaushik, K. Basu, C. Benoit, C. M. Cirtiu, H. Vali, and A. Moores, "Cellulose nanocrystals as chiral inducers: Enantioselective catalysis and transmission electron microscopy 3D characterization," J. Am. Chem. Soc. **137**, 6124–6127 (2015).
[19]L. Onsager, "The effects of shape on the interaction of colloidal particles," Ann. N. Y. Acad. Sci. **51**, 627–659 (1949).
[20]S. D. Lee, "A numerical investigation of nematic ordering based on a simple hard-rod model," J. Chem. Phys. **87**, 4972–4974 (1987).
[21]P. Bolhuis and D. Frenkel, "Tracing the phase boundaries of hard spherocylinders," J. Chem. Phys. **106**, 666–687 (1997).
[22]H. H. Wensink and G. J. Vroege, "Isotropic–nematic phase behavior of length-polydisperse hard rods," J. Chem. Phys. **119**, 6868–6882 (2003); arXiv:0304430 [cond-mat].
[23]J. D. Parsons, "Nematic ordering in a system of rods," Phys. Rev. A **19**, 1225–1230 (1979).
[24]T. Odijk, "Theory of lyotropic polymer liquid crystals," Macromolecules **19**, 2313–2329 (1986).
[25]A. Stroobants, H. N. W. Lekkerkerker, and T. Odijk, "Effect of electrostatic interaction on the liquid crystal phase transition in solutions of rodlike polyelectrolytes," Macromolecules **19**, 2232–2238 (1986).
[26]H. H. Wensink and E. Trizac, "Generalized Onsager theory for strongly anisometric patchy colloids," J. Chem. Phys. **140**, 024901 (2014).
[27]X. M. Dong, T. Kimura, J.-F. Revol, and D. G. Gray, "Effects of ionic strength on the isotropic-chiral nematic phase transition of suspensions of cellulose crystallites," Langmuir **12**, 2076–2082 (1996).
[28]M. M. C. Tortora, G. Mishra, D. Prešern, and J. P. K. Doye, "Chiral shape fluctuations and the origin of chirality in cholesteric phases of DNA origamis," Sci. Adv. **6**, eaaw8331 (2020).
[29]A. B. Harris, R. D. Kamien, and T. C. Lubensky, "Molecular chirality and chiral parameters," Rev. Mod. Phys. **71**, 1745 (1999).
[30]J.-F. Revol and R. H. Marchessault, "*In vitro* chiral nematic ordering of chitin crystallites," Int. J. Biol. Macromol. **15**, 329 (1993).
[31]W. J. Orts, J.-F. Revol, L. Godbout, and R. H. Marchessault, "SANS study of chirality and order in liquid crystalline cellulose suspensions," MRS Online Proc. Libr. Arch. **376**, 317 (1994).
[32]J. Araki and S. Kuga, "Effect of trace electrolyte on liquid crystal type of cellulose microcrystals," Langmuir **17**, 4493–4496 (2001).
[33]J. Araki, M. Wada, and S. Kuga, "Steric stabilization of a cellulose microcrystal suspension by poly(ethylene glycol) grafting," Langmuir **17**, 21–27 (2000).
[34]L. Heux, G. Chauve, and C. Bonini, "Nonflocculating and chiral-nematic self-ordering of cellulose microcrystals suspensions in nonpolar solvents," Langmuir **16**, 8210–8212 (2000).
[35]J. Yi, Q. Xu, X. Zhang, and H. Zhang, "Chiral-nematic self-ordering of rodlike cellulose nanocrystals grafted with poly(styrene) in both thermotropic and lyotropic states," Polymer **49**, 4406–4412 (2008).
[36]A. Kuhnhold and T. Schilling, "Isotropic-nematic transition and cholesteric phases of helical Yukawa rods," J. Chem. Phys. **145**, 194904 (2016).
[37]C. Honorato-Rios, A. Kuhnhold, J. R. Bruckner, R. Dannert, T. Schilling, and J. P. F. Lagerwall, "Equilibrium liquid crystal phase diagrams and detection of kinetic arrest in cellulose nanocrystal suspensions," Front. Mater. **3**, 21 (2016).
[38]J. P. Straley, "Theory of piezoelectricity in nematic liquid crystals, and of the cholesteric ordering," Phys. Rev. A **14**, 1835–1841 (1976).
[39]S. Dussi and M. Dijkstra, "Entropy-driven formation of chiral nematic phases by computer simulations," Nat. Commun. **7**, 11175 (2016).
[40]Z. Zhao, O. E. Shklyaev, A. Nili, M. N. A. Mohamed, J. D. Kubicki, V. H. Crespi, and L. Zhong, "Cellulose microfibril twist, mechanics, and implication for cellulose biosynthesis," J. Phys. Chem. A **117**, 2580–2589 (2013).
[41]J.-F. Revol, D. L. Godbout, and D. G. Gray, "Solid self-assembled films of cellulose with chiral nematic order and optically variable properties," J. Pulp Pap. Sci. **24**, 146 (1998).
[42]L. Chen, Q. Wang, K. Hirth, C. Baez, U. P. Agarwal, and J. Y. Zhu, "Tailoring the yield and characteristics of wood cellulose nanocrystals (CNC) using concentrated acid hydrolysis," Cellulose **22**, 1753 (2015).
[43]S. J. Hanley, J.-F. Revol, L. Godbout, and D. G. Gray, "Atomic force microscopy and transmission electron microscopy of cellulose from Micrasterias denticulata; evidence for a chiral helical microfibril twist," Cellulose **4**, 209–220 (1997).
[44]S. Elazzouzi-Hafraoui, Y. Nishiyama, J.-L. Putaux, L. Heux, F. Dubreuil, and C. Rochas, "The shape and size distribution of crystalline nanoparticles prepared by acid hydrolysis of native cellulose," Biomacromolecules **9**, 57–65 (2008).
[45]M. Khandelwal and A. Windle, "Origin of chiral interactions in cellulose supramolecular microfibrils," Carbohydr. Polym. **106**, 128–131 (2014).
[46]M. Arcari, E. Zuccarella, R. Axelrod, J. Adamcik, A. Sánchez-Ferrer, R. Mezzenga, and G. Nyström, "Nanostructural properties and twist periodicity of cellulose nanofibrils with variable charge density," Biomacromolecules **20**, 1288 (2019).
[47]J. F. Matthews, C. E. Skopec, P. E. Mason, P. Zuccato, R. W. Torget, J. Sugiyama, M. E. Himmel, and J. W. Brady, "Computer simulation studies of microcrystalline cellulose iβ," Carbohydr. Res. **341**, 138–152 (2006).
[48]A. D. French and G. P. Johnson, "Cellulose and the twofold screw axis: Modeling and experimental arguments," Cellulose **16**, 959 (2009).
[49]K. Conley, L. Godbout, M. A. Whitehead, and T. G. M. Van De Ven, "Origin of the twist of cellulosic materials," Carbohydr. Polym. **135**, 285–299 (2016).
[50]A. Paajanen, S. Ceccherini, T. Maloney, and J. A. Ketoja, "Chirality and bound water in the hierarchical cellulose structure," Cellulose **26**, 5877–5892 (2019).
[51]T. Dumitrică, "Intrinsic twist in iβ cellulose microfibrils by tight-binding objective boundary calculations," Carbohydr. Polym. **230**, 115624 (2020).
[52]A. Y. Mehandzhiyski, N. Rolland, M. Garg, J. Wohlert, M. Linares, and I. Zozoulenko, "A novel supra coarse-grained model for cellulose," Cellulose **27**, 4221 (2020).
[53]Y. Habibi, L. A. Lucia, and O. J. Rojas, "Cellulose nanocrystals: Chemistry, self-assembly, and applications," Chem. Rev. **110**, 3479–3500 (2010).
[54]C. Bonini, L. Heux, J.-Y. Cavaillé, P. Lindner, C. Dewhurst, and P. Terech, "Rodlike cellulose whiskers coated with surfactant: A small-angle neutron scattering characterization," Langmuir **18**, 3311–3314 (2002).
[55]S. Elazzouzi-Hafraoui, J.-L. Putaux, and L. Heux, "Self-assembling and chiral nematic properties of organophilic cellulose nanocrystals," J. Phys. Chem. B **113**, 11069–11075 (2009).
[56]B. Frka-Petesic, B. Jean, and L. Heux, "First experimental evidence of a giant permanent electric-dipole moment in cellulose nanocrystals," Europhys. Lett. **107**, 28006 (2014).

[57]T. Odijk, "Pitch of a polymer cholesteric," J. Phys. Chem. **91**, 6060–6062 (1987).
[58]J. Majoinen, J. Hassinen, J. S. Haataja, H. T. Rekola, E. Kontturi, M. A. Kostiainen, R. H. A. Ras, P. Törmä, and O. Ikkala, "Chiral plasmonics using twisting along cellulose nanocrystals as a template for gold nanoparticles," Adv. Mater. **28**, 5262–5267 (2016).
[59]J.-F. Revol, D. L. Godbout, and D. G. Gray, "Solidified liquid crystals of cellulose with optically variable properties," U.S. patent 5,629,055 (May 13, 1997).
[60]S. Beck, J. Bouchard, and R. Berry, "Controlling the reflection wavelength of iridescent solid films of nanocrystalline cellulose," Biomacromolecules **12**, 167–172 (2011).
[61]R. M. Parker, G. Guidetti, C. A. Williams, T. Zhao, A. Narkevicius, S. Vignolini, and B. Frka-Petesic, "The self-assembly of cellulose nanocrystals: Hierarchical design of visual appearance," Adv. Mater. **30**, 1704477 (2018).
[62]C. Honorato-Rios and J. P. F. Lagerwall, "Interrogating helical nanorod self-assembly with fractionated cellulose nanocrystal suspensions," Commun. Mater. **1**, 69 (2020).
[63]C. Honorato-Rios, C. Lehr, C. Schütz, R. Sanctuary, M. A. Osipov, J. Baller, and J. P. F. Lagerwall, "Fractionation of cellulose nanocrystals: Enhancing liquid crystal ordering without promoting gelation," NPG Asia Mater. **10**, 455–465 (2018).
[64]P. Oswald and P. Pieranski, *Nematic and Cholesteric Liquid Crystals: Concepts and Physical Properties Illustrated by Experiments* (CRC Press, Boca Raton, FL, 2005), p. 648.
[65]H. H. Wensink and G. Jackson, "Generalized van der Waals theory for the twist elastic modulus and helical pitch of cholesterics," J. Chem. Phys. **130**, 234911 (2009).
[66]S. Belli, A. Patti, M. Dijkstra, and R. van Roij, "Polydispersity stabilizes biaxial nematic liquid crystals," Phys. Rev. Lett. **107**, 148303 (2011).
[67]H. H. Wensink, "Effect of size polydispersity on the pitch of nanorod cholesterics," Crystals **9**, 143 (2019).
[68]X. M. Dong, J.-F. Revol, and D. G. Gray, "Effect of microcrystallite preparation conditions on the formation of colloid crystals of cellulose," Cellulose **5**, 19–32 (1998).
[69]K. W. Klockars, B. L. Tardy, M. Borghei, A. Tripathi, L. G. Greca, and O. J. Rojas, "Effect of anisotropy of cellulose nanocrystal suspensions on stratification, domain structure formation, and structural colors," Biomacromolecules **19**, 2931–2943 (2018).
[70]R. M. Parker, B. Frka-Petesic, G. Guidetti, G. Kamita, G. Consani, C. Abell, and S. Vignolini, "Hierarchical self-assembly of cellulose nanocrystals in a confined geometry," ACS Nano **10**, 8443–8449 (2016).
[71]B. Zhu, V. E. Johansen, G. Kamita, G. Guidetti, M. M. Bay, T. G. Parton, B. Frka-Petesic, and S. Vignolini, "Hyperspectral imaging of photonic cellulose nanocrystal films: Structure of local defects and implications for self-assembly pathways," ACS Nano **14**, 15361–15373 (2020).
[72]E. Csiszar, P. Kalic, A. Kobol, and E. D. P. Ferreira, "The effect of low frequency ultrasound on the production and properties of nanocrystalline cellulose suspensions and films," Ultrason. Sonochem. **31**, 473–480 (2016).
[73]E. Gicquel, J. Bras, C. Rey, J.-L. Putaux, F. Pignon, B. Jean, and C. Martin, "Impact of sonication on the rheological and colloidal properties of highly concentrated cellulose nanocrystal suspensions," Cellulose **26**, 7619–7634 (2019).
[74]Q. Beuguel, J. R. Tavares, P. J. Carreau, and M.-C. Heuzey, "Ultrasonication of spray- and freeze-dried cellulose nanocrystals in water," J. Colloid Interface Sci. **516**, 23–33 (2018).
[75]A. B. Harris, R. D. Kamien, and T. C. Lubensky, "Microscopic origin of cholesteric pitch," Phys. Rev. Lett. **78**, 1476 (1997).
[76]C. Schütz, J. R. Bruckner, C. Honorato-Rios, Z. Tosheva, M. Anyfantakis, and J. P. F. Lagerwall, "From equilibrium liquid crystal formation and kinetic arrest to photonic bandgap films using suspensions of cellulose nanocrystals," Crystals **10**, 199 (2020).
[77]M. A. Osipov, "Molecular theory of solvent effect on cholesteric ordering in lyotropic polypeptide liquid crystals," Chem. Phys. **96**, 259–270 (1985).
[78]T. G. Parton, G. T. van de Kerkhof, A. Narkevicius, J. S. Haataja, R. M. Parker, B. Frka-Petesic, and S. Vignolini, "Chiral self-assembly of cellulose nanocrystals is driven by crystallite bundles," arXiv:2107.04772 (2021).
[79]W. M. Saslow, M. Gabay, and W.-M. Zhang, "'Spiraling' algorithm: Collective Monte Carlo trial and self-determined boundary conditions for incommensurate spin systems," Phys. Rev. Lett. **68**, 3627–3630 (1992).
[80]M. Collins and W. M. Saslow, "Temperature-dependent pitch and phase diagram for incommensurate XY spins in a slab geometry," Phys. Rev. B **53**, 8533–8538 (1996).
[81]R. Memmer and F. Janssen, "Computer simulation of chiral liquid crystal phases. Part 5: Temperature dependence of the pitch of a cholesteric phase studied under self-determined boundary conditions," J. Chem. Soc., Faraday Trans. **94**, 267–276 (1998).
[82]G. Germano, M. P. Allen, and A. J. Masters, "Simultaneous calculation of the helical pitch and the twist elastic constant in chiral liquid crystals from intermolecular torques," J. Chem. Phys. **116**, 9422–9430 (2002).
[83]S. Růžička and H. H. Wensink, "Simulating the pitch sensitivity of twisted nematics of patchy rods," Soft Matter **12**, 5205–5213 (2016).
[84]S. Varga and G. Jackson, "Simulation of the macroscopic pitch of a chiral nematic phase of a model chiral mesogen," Chem. Phys. Lett. **377**, 6–12 (2003).
[85]M. P. Allen, G. T. Evans, D. Frenkel, and B. M. Mulder, "Hard convex body fluids," in *Advances in Chemical Physics* (John Wiley & Sons, Ltd., 2007), pp. 1–166.